Multi-energy activation of natural krypton

Spectrum-averaged neutron-capture cross sections using six neutron spectra

Jan Butz, Leon Fährnrich, Carolin Grün, Alina Gottschalk, Samira Ikerkourn, Felix Panholzer, Davud Sokolovic, Tanja Heftrich, René Reifarth

Institute for Applied Physics, Experimental Astrophysics Group, Goethe University Frankfurt, Germany

Experimental Astrophysics

GOETHE UNIVERSITÄT FRANKFURT AM MAIN

Abstract ID: #195

Astrophysical Motivation

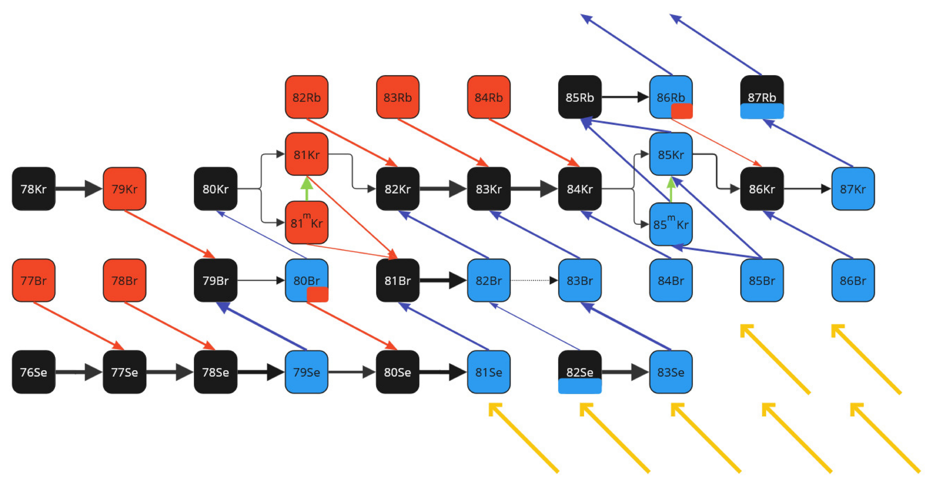

Figure: Neutron-capture paths around the krypton region [3, 7].

- The lower temperature region of the main component lies at approximately $k_B T = 5$–25 keV in AGB stars, while the weak component in massive stars covers approximately $k_B T = 30$–90 keV [1, 2].
- The $^{79}\mathrm{Se}$ branching influences the ratio of the s-only isotopes $^{80}\mathrm{Kr}$ and $^{82}\mathrm{Kr}$, and therefore depends not only on the neutron density but also on the stellar temperature [1].

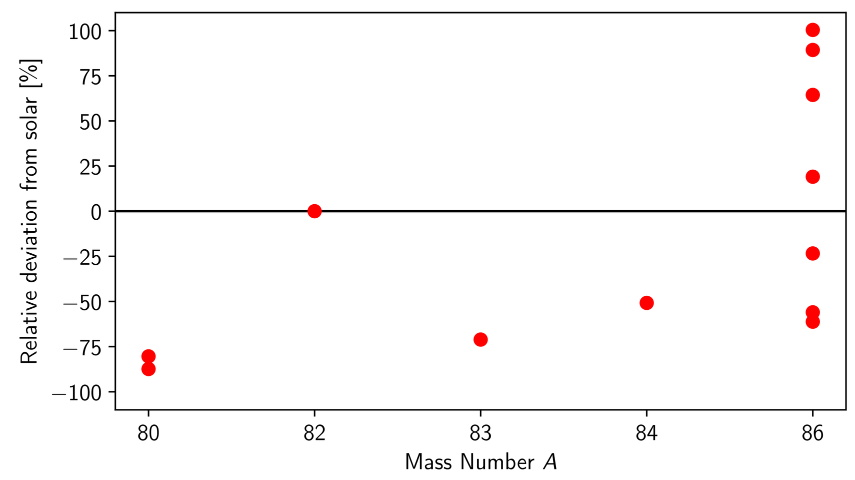

Figure: Ratio of the stable krypton isotopes in presolar SiC grains relative to solar [16–18].

- The $^{85}\mathrm{Kr}$ branching affects the production of $^{86}\mathrm{Kr}$. The $^{86}\mathrm{Kr}/^{82}\mathrm{Kr}$ ratio is therefore sensitive to this branching and to the local neutron density [4, 5].
- The measured abundance spread in the $^{86}\mathrm{Kr}/^{82}\mathrm{Kr}$ ratio changes significantly from one grain to another [16, 17]. In this work, the activation method is applied for the first time to natural krypton at several distinct energies.

Natural Krypton Spheres

Figure: 30 mm sphere secured in the filling adapter [7].

- Special spherical gas targets had already been developed by Rupp *et al.* [6] at KIT for ToF measurements. Since only sketches and the spheres themselves were available, new technical drawings and tools were produced with the help of the IAP workshop.
- The new spheres consist of 0.5 mm stainless steel, were laser welded and leak tested, and have an inner radius of 14.44 mm.
- They were filled with 99.99 % natural krypton.

Table: Isotopic abundances I and molar masses M used in the analysis [8].

isotope	I (%)	M (g/mol)
$^{78}\mathrm{Kr}$	0.355 ± 0.003	77.920366 ± 0.000002
$^{84}\mathrm{Kr}$	56.987 ± 0.015	$83.91149773 \pm 0.00000003$
$^{86}\mathrm{Kr}$	17.279 ± 0.041	$85.91061063 \pm 0.00000003$

Neutron Production and NEW GENESYS

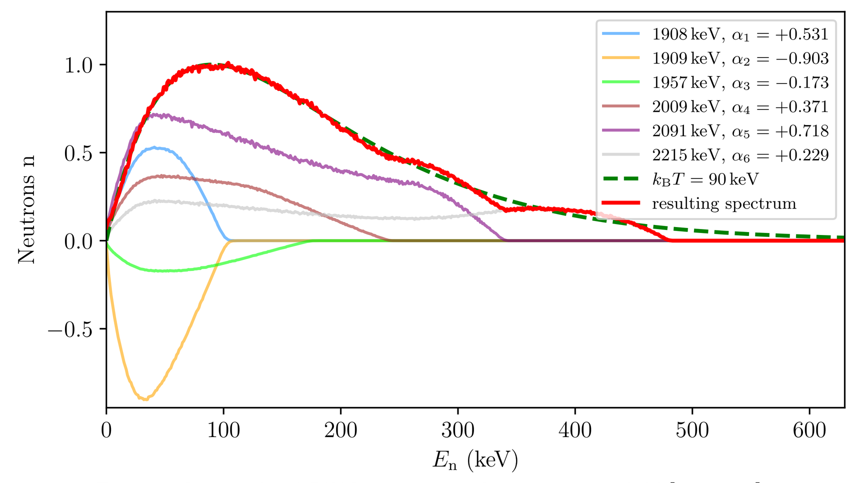

Figure: Six weighted PINO spectra for $k_B T = 90$ keV [7, 9, 10].

Six different proton energies and sample distances were used to obtain the required neutron spectra through a linear combination. PINO [9] was used to simulate the individual neutron spectra. NEW GENESYS [10], developed by P. Erbacher and modernised in this work, selects the necessary sub-spectra and calculates the weighting factors.

Table: Proton energies and sample distances of the six neutron fields [7].

sub-spectrum	E_p (keV)	d (mm)
1	1908	23.5
2	1909	16.0
3	1957	16.0
4	2009	16.0
5	2091	21.5
6	2215	17.0

SACS and almost MACS

For each sub-spectrum the SACS σ_i was obtained. The β_i values were then used to calculate the almost MACS.

$$\sigma_{\mathrm{SACS}} = \frac{\int \sigma(E)\Phi(E)\,dE}{\int \Phi(E)\,dE},$$

$$\sigma_i = \frac{\int \sigma_i(E)\Phi_i(E)\,dE}{\int \Phi_i(E)\,dE},$$

$$\sigma_{\mathrm{MACS}}^{\mathrm{al}} = \frac{2}{\sqrt{\pi}} \sum_i \beta_i \sigma_{i,\mathrm{SACS}}.$$

Experimental Setup and Sample Holder

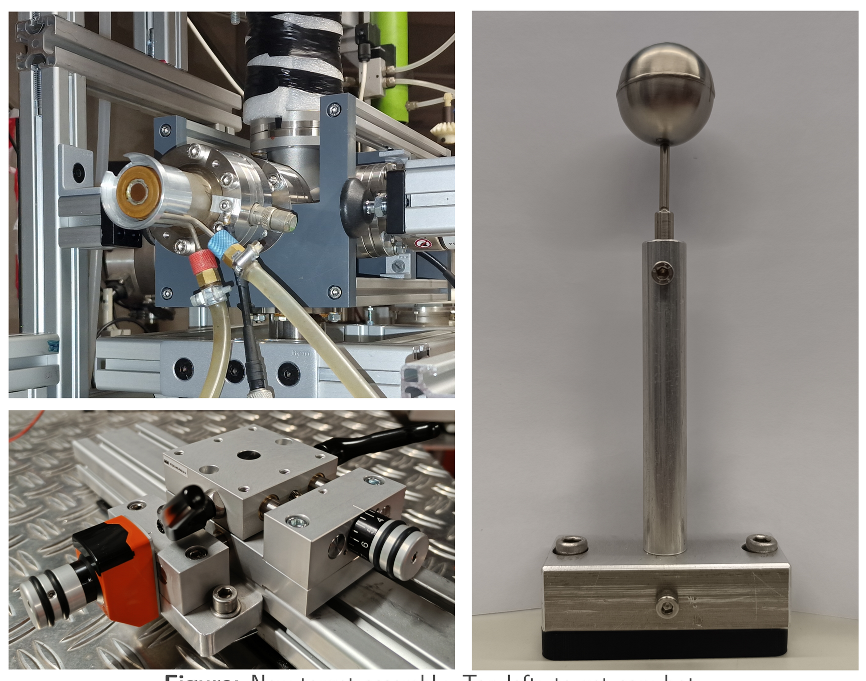

Figure: New target assembly. Top left: target cap; bottom left: cross table; right: new sample holder [7].

- The activations were performed with a 2.5 MeV Van de Graaff accelerator using the $^7\mathrm{Li}(\mathrm{p,n})^7\mathrm{Be}$ reaction, a 100 µm lithium layer and a proton-beam radius of 1.5 mm.
- For the spherical samples, a new target assembly was developed. The cross table allows continuous adjustment of the sample position. The modular sample holder was developed for spherical samples, while an adapter can also be mounted for solid-state matter samples.
- A Li-glass detector monitored the neutron-flux stability during the activation.

Activation and Analysis

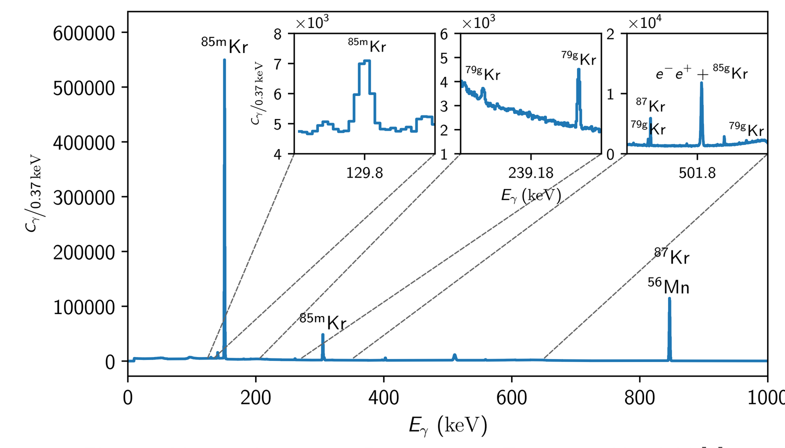

Figure: Measured spectrum Detector 1 at $E_p = 2215$ keV [7].

The spheres were measured with a BEGe detector setup. The activated nuclei N_{act} were calculated from the measured counts C_γ with dead-time and detector-efficiency corrections.

Neutron monitor

$^{86}\mathrm{Kr}$ was used as the neutron-flux monitor. Its SACS was calculated with PINO [9] using ENDF/B-VIII.1 [11] after comparison with Mutti *et al.* [5] and Tessler *et al.* [15]. A systematic uncertainty of 3 % was applied.

Table: Populated krypton states and their treatment in this work [7].

reaction	treatment in this work
$^{78}\mathrm{Kr}(\mathrm{n},\gamma)\ ^{79}\mathrm{Kr}$	The isomeric state was not observed separately. The result corresponds to total $^{79}\mathrm{Kr}$.
$^{80}\mathrm{Kr}(\mathrm{n},\gamma)\ ^{81m,g}\mathrm{Kr}$	Neither state could be determined with the applied decay counting.
$^{84}\mathrm{Kr}(\mathrm{n},\gamma)\ ^{85m,g}\mathrm{Kr}$	The $^{85m}\mathrm{Kr}$ result is shown. The $^{85g}\mathrm{Kr}$ result requires re-evaluation.
$^{86}\mathrm{Kr}(\mathrm{n},\gamma)\ ^{87}\mathrm{Kr}$	Internal neutron-flux monitor.

Internal normalisation

Particle ratios r_N from activated and parent nuclei give the χ values relative to $^{86}\mathrm{Kr}$, from which the SACS are obtained. This allows re-evaluation if the $^{86}\mathrm{Kr}$ cross section is updated:

$$r_N = \frac{^{A+1}N}{^{A}N}, \qquad \chi = \frac{r_N^{x\mathrm{Kr}}}{r_N^{86\mathrm{Kr}}},$$

$$\sigma^{x\mathrm{Kr}} = \frac{r_N^{x\mathrm{Kr}}}{r_N^{86\mathrm{Kr}}}\sigma^{86\mathrm{Kr}} = \chi\,\sigma^{86\mathrm{Kr}}.$$

Results: SACS and almost MACS

The SACS uncertainty ranges correspond to $\pm 2\sigma$. The almost MACS is calculated from the values determined with the modernised NEW GENESYS [10] tool.

$^{78}\mathrm{Kr}(\mathrm{n},\gamma)\ ^{79}\mathrm{Kr}$

The isomeric state of $^{79}\mathrm{Kr}$ was not observed separately. The result therefore corresponds to total $^{79}\mathrm{Kr}$. The SACS is compared with ENDF/B-VIII.1, JEFF-3.3, JEFF-4 and TENDL-2019 [11–14]; the almost MACS with Tessler *et al.* [15].

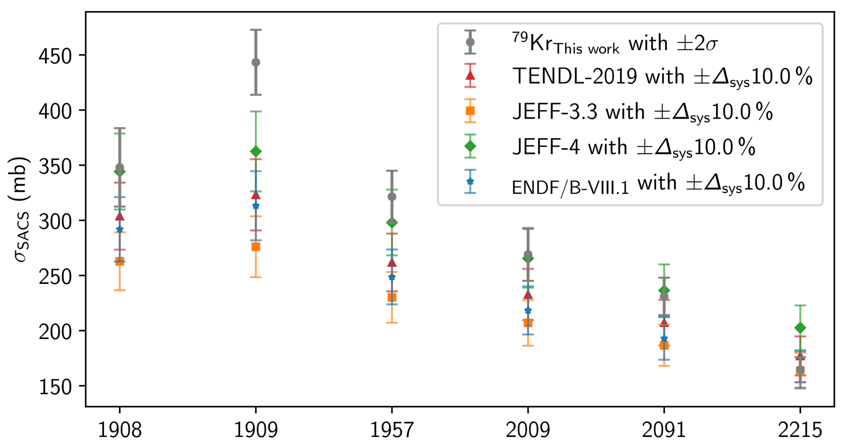

Figure: SACS from this work [7] with ENDF/B-VIII.1, JEFF-3.3, JEFF-4 and TENDL-2019 [11–14].

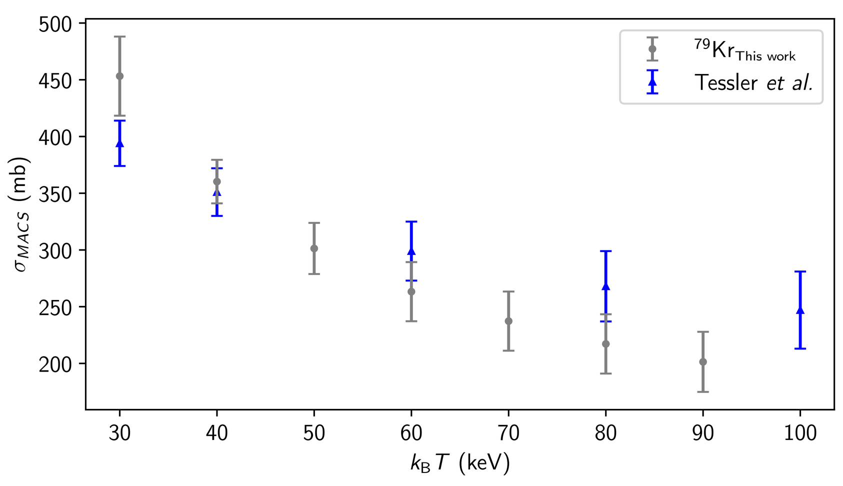

Figure: Almost MACS from this work [7, 10] and Tessler *et al.* [15].

$^{84}\mathrm{Kr}(\mathrm{n},\gamma)\ ^{85m}\mathrm{Kr}$

The $^{85m}\mathrm{Kr}$ result is shown, while the $^{85g}\mathrm{Kr}$ result requires re-evaluation. The SACS is compared with JEFF-3.3, JEFF-4 and TENDL-2019 [12–14]; the almost MACS with Tessler *et al.* [15].

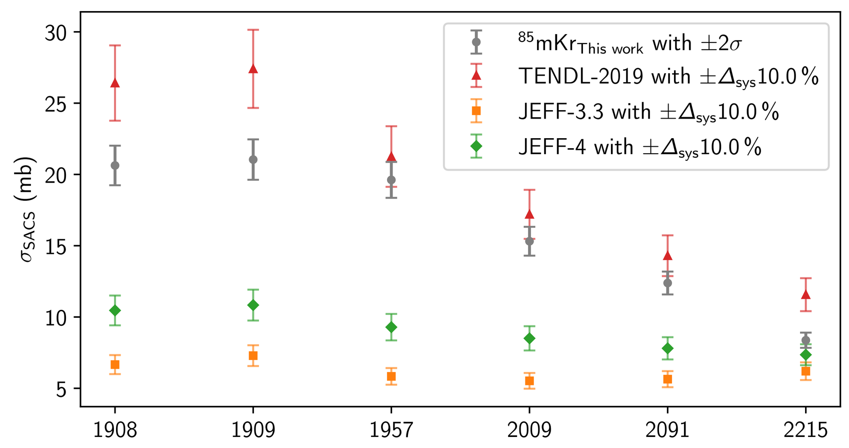

Figure: SACS from this work [7] with JEFF-3.3, JEFF-4 and TENDL-2019 [12–14].

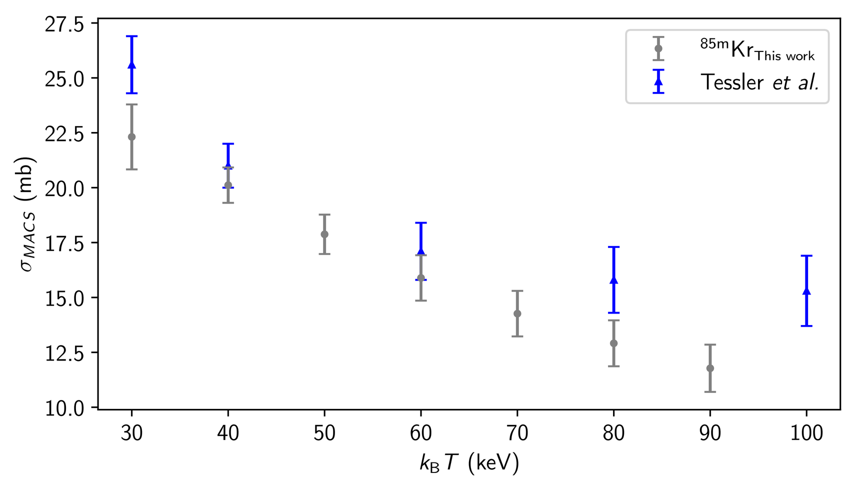

Figure: Almost MACS from this work [7, 10] and Tessler *et al.* [15].

Outlook

Analysis

- Re-evaluate $^{84}\mathrm{Kr}(\mathrm{n},\gamma)\ ^{85g}\mathrm{Kr}$, as this showed the largest difference from the literature and was also inconsistent within the measurement campaign itself.
- Re-check the naturally occurring $^{85g}\mathrm{Kr}$ background and investigate inaccessible channels with atom-counting methods, including atom trap trace analysis for the long-lived krypton isotopes.
- Re-evaluate the other investigated isotopes when new and more precise measurements of the $^{86}\mathrm{Kr}$ monitor are published, especially if the data are taken with the ToF method.

Experimental setup

- Check the setup in future to ensure that the digital display accurately reflects the sample position. An activation study should be carried out using the gold-standard as a reference.
- Reduce the sphere wall thickness to reduce scattering and neutron energy loss in the outer wall, and remove excessive welding in the equator region.

References: **[1]** R. Reifarth, C. Lederer and F. Käppeler, J. Phys. G 41 (2014) 053101. **[2]** M. Pignatari et al., Astrophys. J. 710 (2010) 1557. **[3]** J. Magill, G. Pfennig and J. Galy, *Karlsruher Nuklidkarte*, 7th ed. (2007). **[4]** S. Fiebiger, Ph.D. thesis, Goethe-Universität Frankfurt (2018). **[5]** P. Mutti et al., AIP Conf. Proc. 769 (2005) 1327–1330. **[6]** G. Rupp et al., Nucl. Instrum. Methods A 608 (2009) 152–156. **[7]** J. Butz, M.Sc. thesis, Goethe University Frankfurt (2025). **[8]** J. R. de Laeter et al., Pure Appl. Chem. 75 (2003) 683–800. **[9]** R. Reifarth et al., Nucl. Instrum. Methods A 608 (2009) 139–143. **[10]** P. Erbacher, *90 keV Method*, IAP Technical Report (2020). **[11]** G. P. A. Nobre et al., *ENDF/B-VIII.1* (2024). **[12]** A. J. M. Plompen et al., Eur. Phys. J. A 56 (2020) 181. **[13]** OECD NEA Data Bank, *JEFF-4.0* (2025). **[14]** A. J. Koning et al., Nucl. Data Sheets 155 (2019) 1–55. **[15]** M. Tessler et al., Phys. Rev. C 104 (2021) 015806. **[16]** M. Pignatari et al., Mem. Soc. Astron. Ital. 77 (2006) 897–902. **[17]** R. S. Lewis, S. Amari and E. Anders, Geochim. Cosmochim. Acta 58 (1994) 471–494. **[18]** K. Lodders, Astrophys. J. 591 (2003) 1220–1247.